Laser Speckle Interferometry
Applied to the Measurement of
Gun-tube Motion During Firing

by

Piyush K. Gupta and F.P. Chiang
Laboratory for Experimental Mechanics Research,
State University of New York at Stony Brook,
Stony Brook, NY 11794-2300.

1 Introduction

Experimental investigation into the motion of gun-tubes has been pursued by many researchers using various techniques. Pilcher *et al* [1] have used accelerometers to measure the gun-tube motion during the interior ballistic cycle. They obtained velocity and displacement data by integrating the data for acceleration. Simkins *et al* have obtained corroborative measurements of the transverse motion of a gun-tube during firing using eddy-current probes and optrons. [2] They have cross-compared the measurements by the two techniques and have found them to be in close agreement with each other. However, they have measured the transverse motion of the gun-tube, six inches rearward of the muzzle. Further, these probes detect transverse motion at a particular point in spatial and not material co-ordinates. The probes do not translate as the gun recoils. Consequently, they measure the transverse motion at different *material* points along the gun-tube as the gun recoils. Hence, they are incapable of showing the spatial modes of the oscillation. It has been recognized that as opposed to the transverse position of the muzzle, the slope of gun-tube axis and the transverse velocity of the muzzle are more significant factors contributing towards the accuracy of a ballistic projectile. [4]

Efforts were therefore directed towards developing a technique which could yield whole field displacement information at the gun muzzle. With a whole field displacement information at hand, it would be possible to detect the spatial modes of oscillation of the gun-tube. Further, measuring transverse vibrations of large caliber gun-tubes, like those of tank-guns, using

accelerometers and eddy-probes or optrons is difficult because the pressure waves generated by the escaping powder gases are powerful enough to damage any measuring devices in close proximity of the muzzle. There exists, therefore, a need to develop a *remote sensing, precise enough* technique which can yield *whole-field* information. One such technique is laser speckle interferometry which we have used earlier to measure the transient transverse vibrations of a cantilever beam after impact [3]. As the next step towards applying this technique to the measurement of transverse vibrations of large caliber gun-tubes, we have herein successfully applied laser speckle interferometry to study the motion of a 20 *mm* gun-tube. We have determined its transverse, radial and twisting motions. Being an optical technique, it is remote sensing and it does not require attachment of any instrumentation in the immediate vicinity of the muzzle. It yields whole-field information as well. The advantages and drawbacks of this technique and the sources and magnitude of error are identified in order to get an insight into the feasibility of applying this technique to study tank-gun vibrations.

2 Experimental Method

In this section, we briefly discuss the underlying principles of laser speckle interferometry. We also present the governing equations for applying this technique to measuring in-plane displacement.

Burch and Tokaski [6] were the first investigators to observe and formulate the basic principles of laser speckle interferometry. This technique was first extended to the measurement of displacement by Burch *et al* in 1970 and

1972 [7,8]. Since then a variety of methods based on the same basic principle have been developed. Chiang [9] has presented a unified approach to all of these techniques treating speckle displacement as a general phenomenon.

Khetan and Chiang [10] have derived the governing mathematical relationships for one beam laser speckle interferometry.

2.1 Measurement of In-plane Displacement by Double Exposure Speckle Interferometry

Double exposure speckle photography can be applied to the measurement of displacement in the plane normal to the line of sight by recording with a camera two superimposed images of a surface, at two different instants of time. The displacement of the surface within this time interval can be obtained as discussed below.

The surface is illuminated by coherent light from a laser. The speckle pattern thus generated gets recorded on the film. To facilitate the formation of a good speckle field, the surface is sprayed sparingly with flat white paint giving it a white and dark granular appearance. A slow film like $Agfa10E75$ is used because it has a small grain size which is essential to capture the fine speckle field and also to differentiate its movement between the two exposures. Because the film grain is fine, a large exposure time or a high intensity illumination is required. For studying displacements following static loading one can conveniently apply a low power laser and expose the film for a long time. With a 5 mW He-Ne laser a three minute exposure is not uncommon. Obviously, within this time the whole set-up should not move beyond the least detectable limit. Hence, for such experiments, vibration isolated tables

3

are an essential requirement. On the other hand, for capturing instants while studying dynamic displacement, a pulsed laser emitting radiation in the optical region finds application. Usually a pulsed ruby laser is very befitting for such applications because it emits pulses which are 20 to 30 *nanoseconds* (*ns*) long and emission is in the red region of the optical spectrum which also is the region in which *Agfa*10E75 is sensitive. If the movement of the image between two exposures is larger than the diameter of the speckles and furthermore if the speckles remain correlated with one another then any area of the image will scatter a beam of light into a diffraction halo whose intensity will vary periodically across the field yielding cosine square fringes. These fringes will have an angular spacing α which is related to the wavelength λ of the readout beam, m the demagnification factor of the image and the surface displacement D by the following relation [9,10].

$$\sin \alpha = \frac{\lambda m}{D} \tag{1}$$

The direction of the fringes will be orthogonal to the direction of the displacement. (See Figure (1)).

The camera is placed as normal to the surface as possible to eliminate the effects of the out-of-plane displacements. The selection of the distance at which the camera should be placed from the surface whose displacement has to be determined depends upon the range of displacement to be captured which in turn also limits the magnitude of the smallest detectable displacement. Thus, higher demagnification results in a larger range of measurable displacement but poorer sensitivity. The speckle diameter on the object (Σ)

is [9,10] :

$$\Sigma = 1.2m\lambda F \tag{2}$$

Surface displacements of magnitude greater than this are therefore measurable. The maximum detectable displacement is limited by the ability to resolve or count the fringes in the halo. More than 20 fringes pose a problem unless the fringe quality is excellent.

2.2 Experimental Setup and Procedure

Since we are interested in determining the displacement of the gun-tube muzzle at successive instants of time from the instant the round is fired by double exposure speckle interferometry, we have used a pulsed ruby laser to illuminate the gun-tube muzzle.

Figure (3) shows the location of the camera with respect to the gun-tube. Its focal length f is 55 mm and it uses a 4 $in.\times$ 5 $in.$ film. For our experiments we have used the $Agfa10E75$ film. The aperture of the camera is set at $f/4.7$ (or $F=4.7$). The laser beam from the pulsed ruby laser, expanded using a concave lens, illuminates the area around the gun-tube muzzle with intensity sufficient to expose the film within its pulse width time of 30 ns. In our case the maximum displacements are of the order of 600 μm. In our setup demagnification $m = 5.34$ is obtained and hence using equation (2) we obtain a sensitivity of about 19.4 μm as the smallest detectable displacement. The specklegrams are read by the point-wise technique at the gun-tube muzzle using a He-Ne laser. The farfield diffraction pattern is observed at a distance $l = 0.72$ m from the specklegram. The halo of diameter $d = 0.15$ m is observed and n, the number of bright fringes across a distance d' within

5

the halo are counted. The angular spacing of the fringes is estimated using equation (3).

$$\sin \alpha = \frac{d'}{nl} \tag{3}$$

Using equations (1) and (3), the object displacement per bright fringe is found to be 15.9 μm.

Figure (2) shows the dimensions of the gun-tube. The gun-tube is 152.4 cm long. A number of authors have noted that minimum shot to shot dispersion is obtained when the gun-tube is suspended by steel wires and is free to recoil. [4,5] But in our case, we could not allow free recoil. Unlike the sandwich laser speckle technique, in our setup, we are recording the two relatively displaced speckle fields on the same photographic film. Hence, in our case, laser speckle interferometry can be applied only if the magnitude of the displacements in the both x and y directions are of the same order. This is evident from the discussion of maximum and minimum measurable displacement following equation (2). Hence, the gun-tube is clamped using two clamps, each 5 cm wide, and approximately 22 cm apart. The rear clamp restricts the axial movement of the gun-tube. The gun-tube overhangs 108.9 cm ahead of the front clamp and 11.7 cm behind the rear clamp. Both the clamps are mounted on a steel base 90 cm long, 15 cm wide and 5 cm thick. The front end of the metal base is hinged to another metal slab 100 cm long, 30 cm wide and 7.5 cm thick under it, which in turn is clamped to two I-section metal rails, 46 cm high and 210 cm long. These rails are clamped to 2.5 cm thick metal plates bolted on to the floor covering an area 90 cm wide and 250 cm in length. The rear end of the metal base is gripped by friction

6

1000 μs, the recoil is of a magnitude large enough to result in a decorrelation of the superimposed speckle fields. Hence, beyond a delay of 1000 μs after firing, the laser is operated in the double pulse mode. It emits two pulses, 20 μs apart. Thus the differential displacement within this short time interval of 20 μs, after an initial preset delay of 1000 μs and more, generates the two superimposed correlated speckle fields within a single exposure. The initial delay is then varied in steps of 20 μs from 1000 μs to 2400 μs. The projectile spends about 2300 μs within the gun-tube. The absolute displacement at each instant is calculated by catenating the differential displacements back-to-back.

The signal from the strain gages following the firing is found to be similar for all the 200 repetitions of the process. This substantiates the repeatability of the experiment which is an essential requirement and assumption in applying this technique to construct the displacement versus time curve, point-by-point.

Each of the specklegrams obtained is marked and coded and all the temporal information is noted down from the oscilloscope. Efforts are made to ensure that a time-wise overlap is obtained between the specklegrams containing the differential displacement information.

3   Data Analysis

3.1   Collection of the Raw Data

The specklegrams obtained as discussed above are read by the point-wise technique. The setup to read the fringes as shown in Figure (1) consists

of an electronically indexed $x - y$ translation stage, a 5 mW He-Ne laser, and a rotating screen made of graph paper to read the distance between the fringes correct to 1 mm, with angular markings on the rim to read the orientation of the fringes correct to 1 *degree*. Using this setup, each of the 200 specklegrams is read at 20 different locations at the muzzle. Shown in Figure (5), are the 20 locations at the gun-tube muzzle where the specklegrams are read. For ease of reference, they have been indexed and are referred to by a pair (i, j), where $i = 1, 4$ is the x location index and $j = 1, 5$ is the y location index. Typical fringes obtained after point-wise-readout showing the differential displacement at these 20 different locations at the gun-tube muzzle at a given instant of time after firing are shown in Figure (6).

3.2 Processing of the Raw Data

The fringe spacing, the orientation of the fringes at each location and the time data for each specklegram indicating the preset delay and the interpulse separation in case of the double pulse single exposure type of specklegrams are tabulated and entered into a computer for further processing. The bullet does not spend the same time for each shot within the gun-tube. A jitter of around 100 μs is observed between shot to shot. This can be attributed to inconsistent burning of the charge. In our analysis, we have assumed that the projectile is released from the casing only when sufficient pressure is built within it and the inconsistency in the burning of the charge occurs in this initial phase. Hence, this jitter occurs prior to the release of the projectile from the casing and thereafter the time of travel of the projectile within the gun-tube is identical for all the shots. The time of exit of the

9

bullet from the gun-tube is taken as $t = 0$. The data is rearranged timewise and the displacement in μm is computed using all the parameters of the experimental setup and the relevant relations. (Equations (1) and (3)). The data is thus converted into displacement and orientation readings for each point. Assuming that the displacement in the x direction is always in the direction of recoil, the magnitude and direction of the y component of the displacement is computed.

Since most of the data at any given location contains information about the differential and not the absolute y displacement, (both magnitude and direction) we have developed Fortran codes to construct the absolute y displacement curves at any location. This is discussed below.

To begin with, we have 10 single pulse double exposure specklegrams which provide the initial absolute values of the displacement. The data analysis for this part remains akin to that done for the cantilever beam. [3] Subsequently, we have 160 double pulse specklegrams which give the differential displacements starting at a particular time and the time interval between the two pulses is known. (Out of the 200 specklegrams, 10 specklegrams have static displacement readings to verify our calibration and computation of displacement values, 10 specklegrams provide the absolute displacement readings, and 20 specklegrams have some problem or the other, for eg. developing error, very poor fringes which could not be read etc.) Inspite of attempts made during the experiment to obtain a timewise overlap between this set of 160 specklegrams, we have 12 subsets of specklegrams and within each subset there is a timewise overlap. Thus, in the final data we have 12 gaps in time; less than 5 μs between 8 subsets and less than 80 μs between

10

5 subsets. Therefore, we first construct the displacement curve assuming a zero initial value for a given subset and then join all the subsets together by an extrapolation technique to give the final displacement curves at each of the 20 points.

To construct the displacement curve within a subset, we have developed a Fortran code using a combination of various interpolation routines; some special interpolation routines are written while others from the IMSL library are used. To test our Fortran code, a data set is constructed from a known arbitrary displacement curve, similar in its nature and magnitude to those we anticipate from our experimental data. We use our program to reconstruct this displacement curve from the data set. The error between the reconstructed and the original curve is found to be random in nature. Further, the standard deviation is found to be of the same magnitude as the least detectable displacement by the speckle technique. (See Figure (7)).

From the subset curves thus constructed, the displacement values at regular time intervals within the subsets are extracted. Thus, the data from the 12 subsets is converted into 12 time series which need to be catenated. Judging from the nature of these time series, we fit a single frequency periodic model with a linear trend. We therefore have for each subset the following model.

$$y = A \cos \omega t + B \sin \omega t + a + bt + \epsilon_t \tag{4}$$

Here, a and b are the linear trend parameters, ϵ_t is the error term and A and B are the parameters of a single frequency (ω) periodic model. The principal frequency is estimated by locating the maximum of the squared amplitude

11

periodogram. This involves taking the discrete Fast Fourier Transform of the stationary series. Stationarity is induced in the series by subtracting the linear trend. The parameters for the linear trend are estimated by the method of least squares. Using the estimate of the principal frequency obtained above, and using $A = 0.0$ and $B = 0.0$ as the initial estimates of the Fourier sine and cosine coefficients, the fitted Fourier sine and cosine coefficients are estimated. Thus, the parameters of the assumed model are evaluated and a forecast for a future value of time is obtained. To minimize the error, we forecast the first series and backcast the second series to link them midway between the gap. The Fortran codes used to perform the Fast Fourier Transform and fit the single frequency model are adapted from Bloomfield. [11]

In this way, the y displacement curves at each of the 20 locations are obtained. Each of these curves is converted into a single time series. We thus have 20 curves showing the absolute y displacement versus time at the 20 locations at the muzzle.

3.3 Resolution of Total y- Displacement into Components

Figure (8) shows the choice of the coordinate system. The three motions at the gun-tube muzzle that contribute toward the total y displacement observed at the plane at which the camera is focused are (1) transverse motion : y_t (2) radial expansion of the gun-tube : y_r and (3) surface displacement due to the twisting of the gun-tube about the x-axis : Tw.

We now derive the relation governing the contributions of all these factors

12

toward total speckle displacement in the y direction at the plane at which the camera is focused.

Let d_{fp} be the distance between the x axis and the plane at which the camera is focused. (See Figure (9)).

Consider the points on the surface of the gun-tube lying above the origin. For points on the surface of the gun-tube lying to left of the focus plane we can write

$$y = y_t + y_r \sin \phi + (R+y_r)\theta \cos \phi - \{(R+y_r) \cos \phi 2\theta - (R+y_r) \sin \phi 2\theta^2 - d^l_{fp}2\theta\}$$
(5)

which rearranges into

$$y = y_t + y_r \sin \phi - (R+y_r)\theta \cos \phi + (R+y_r) \sin \phi 2\theta^2 + d^l_{fp}2\theta.$$
(6)

And for points to the right of the plane at which the camera is focused, we have

$$y = y_t + y_r \sin \phi + (R+y_r)\theta \cos \phi + \{-(R+y_r) \cos \phi 2\theta + (R+y_r) \sin \phi 2\theta^2 + d^r_{fp}2\theta\}$$
(7)

which rearranges into

$$y = y_t + y_r \sin \phi - (R+y_r)\theta \cos \phi + (R+y_r) \sin \phi 2\theta^2 + d^r_{fp}2\theta.$$
(8)

Similarly, for points below the origin and to the left of the focus plane, we can write

$$y = y_t - y_r \sin \phi' + (R+y_r)\theta \cos \phi' - \{(R+y_r) \cos \phi' 2\theta + (R+y_r) \sin \phi' 2\theta^2 - d^l_{fp}2\theta\}$$
(9)

13

which rearranges into

$$y = y_t - y_r \sin \phi' - (R + y_r)\theta \cos \phi' - (R + y_r) \sin \phi' 2\theta^2 + d_{fp}^l 2\theta. \qquad (10)$$

And for points to the right of the plane at which the camera is focused, we have

$$y = y_t - y_r \sin \phi' + (R + y_r)\theta \cos \phi' + \{-(R + y_r) \cos \phi' 2\theta - (R + y_r) \sin \phi' 2\theta^2 + d_{fp}^r 2\theta\}$$
$$(11)$$

which rearranges into

$$y = y_t - y_r \sin \phi' - (R + y_r)\theta \cos \phi' - (R + y_r) \sin \phi' 2\theta^2 + d_{fp}^r 2\theta. \qquad (12)$$

But since $\phi' = 2\pi - \phi$, we have $\phi' = -\phi$, $d_{fp}^l = d_{fp}^r = d_{fp}$, and assuming $y_r << R$, we can write $(R + y_r) \approx R$, where R is the radius of the gun-tube. Thus, we can re-write equations (6), (8), (10) and (12) as

$$y = (y_t + 2d_{fp}\theta) + \sin \phi(2y_r + 2R\theta^2) + \cos \phi(-R\theta). \qquad (13)$$

The angle ϕ is independent of i and from the indexing settings used on the $x - y$ translation stage while reading the specklegrams, for each j the values of $\sin \phi$ are as shown in Table 1.

Equation (13) governs the total y displacement recorded on the speckle-gram at any point (i, j). For a given i, we can select any three values of j to obtain a system of three linear equations with the three coefficients shown within brackets in equation (13) as the three unknowns. To minimize computational error, we select $j = 1, 3, \& \ 5$ for our computations for $i = 1, 2, \& \ 3$. For $i = 4$, the data at point $(4, 3)$ is not found to be reliable. Hence for

14

Table 1: Values of $\sin\phi$ for different points (i, j)

$\sin\phi_{(i,1)}$	1.0
$\sin\phi_{(i,2)}$	500.0/950.0
$\sin\phi_{(i,3)}$	50.0/950.0
$\sin\phi_{(i,4)}$	$-400.0/950.0$
$\sin\phi_{(i,5)}$	$-850.0/950.0$

$i = 4$, we select $j = 1, 4, \& 5$ instead. By solving this system of three linear equations, we estimate the twist effect $Tw = R\theta$ from the coefficient of the *cosine* term $(-R\theta)$ in equation (13). Then, knowing R, $R\theta$ and $(y_r + R\theta^2)$ as the coefficient of the *sine* term, we evaluate y_r. Further, the camera is focused at a distance $d_{fp} = R/2$; hence, knowing $R\theta$, we evaluate y_t. Further, note that at $\phi = 0$, $y = y_t$. Hence, if we analyze the specklegrams at $\phi = 0$, we can directly obtain the average instantaneous transverse velocity of the muzzle at any instant by dividing the differential displacement at that instant by the interpulse time separation.

A numerical error analysis is performed on the results for y_t, y_r and Tw. Least counts of various measuring instruments used and the numerical error of interpolation is considered. The mathematical expressions for the computation of error are quite lengthy and omitted for sake of brevity.

3.4 Results

In figures (10) through (21)we present the results for the transverse displacement, radial expansion and the twist effect on the surface in *microns*. The numerically computed limits of error in our results are indicated on the

15

curves.

Owing to the nature of the clamping of the gun-tube in our setup, we obtain a large rotation about the hinge of the metal base causing the muzzle to displace downwards. Hence the displacement curves obtained are not comparable to those obtained by Simkins *et al* [2] for a free recoil boundary condition on the gun-tube.

Using the results for transverse displacement, we have constructed the transverse mode shapes at instants prior to and at projectile exit $(t = 0)$ which are shown in Figure (22). The slope of the muzzle at $t = 0$ can be estimated using the centered difference approximation for y data at $t = 0$. We have,

$$\frac{\partial y}{\partial x} = \frac{y_{(1,j)} - y_{(3,j)}}{2h}$$

where $h = 6781.8 \ \mu m$ is the distance between any points (m,n) and $(m{+}1,n)$. Using the above relation, the average instantaneous slope at the muzzle at $t = 0$ is found to be -0.03510135. Further, applying equation (13) to the differential displacement at muzzle, the average instantaneous transverse velocity of the muzzle at $t = 0$ is found to be $+1.96 \ m/s$.

4   Conclusion

Repeated application of laser speckle interferometry to resolve the twist effect, transverse and radial displacement curves is tedious, time consuming and for large caliber guns, it can be quite expensive in terms of the cost of ammunition required. The construction of the total displacement curve from differential displacement data is prone to significant errors as well.

16

But on the other hand, the transverse muzzle velocity can be obtained by double pulse single exposure laser speckle interferometry by firing only one round and triggering the experiment at the instant the projectile appears at the muzzle by using some kind of detector, for example, snapping cross-wires or an optical obstruction switch. The gun can be allowed to recoil freely if we use the sandwich laser speckle technique. It can also be extended to recordings at a number of instants *within a single firing* using a continuously pulsing laser, like the Copper Vapor Laser. By placing another camera orthoganally, the lateral drift velocity of the muzzle can also be obtained simultaneously. Also, laser speckle interferometry is not restricted to horizontal firings only.

In conclusion, this preliminary study of a 20 *mm* gun-tube using laser speckle interferometry leads us to believe that this technique holds great promise for studying large caliber gun-tubes. Corroborative measurements need to be made to compare the results with those obtained by existing techniques under identical boundary conditions at the gun-tube.

5   Acknowledgment

References

[1] PILCHER, J.O., HENRY, C.L. and MURRAY, R.B., *"Application of Accelerometers for the Measurement of Gun Tube Motion"*, Proceedings, First Conference On: Dynamics of Precision Gun Weapons, Jan. 1977, pp 497-513.

[2] SIMKINS, T.E., PFLEGL, G.A. and SCANLON, R.D., *" Corroborative Measurements of the Transverse Motion of a Gun Tube During Firing"*, Proceedings of the Fourth US Army Symposium on Gun Dynamics, Vol. II, pp IV-1 - IV-16, May 1985.

[3] GUPTA, P.K. and CHIANG, F.P., *"Laser Speckle Interferometry Applied to the Study of Transient Vibrations of a Cantilever Beam"*, Technical Report No. 507, College of Engineering and Applied Sciences, SUNY, Stony Brook, NY 11794, March 1988.

[4] CRANZ, C., *"Cranz's Textbook of Ballistics"*, (Translated by C.C. Bramble *et al*), Vol. III, Second Edition (1927), National Defense Research Committee, 1945.

[5] SNECK, H.J. and GAST, R., *" Normal Mode Analysis of Gun Tube Dynamics"*, Proceedings of the Fourth US Army Symposium on Gun Dynamics, Vol. I, pp I-22 - I-50, May 1985.

[6] BURCH, J.M. and TOKASKI, J.M.J.,"Production of Multiple Beam Fringes from Photographic Scatterers", *Optica Acta*, Vol.15, No.2, 1968.

19

[7] ARCHBOLD, E., BURCH, J.M. and ENNOS, A.E., "Recording of In-plane Surface Displacement by Double Exposure Speckle Holography", *Optica Acta*, Vol.17, No.12, 1970.

[8] ARCHBOLD, E. and ENNOS, A.E., "Displacement Measurement from Double Exposure Laser Photographs", *Optica Acta*, Vol.19, No. 4, 1972.

[9] CHIANG, F.P., "A New Family of 2D and 3D Experimental Stress Analysis Techniques Using Laser Speckles", *SM Archives*, Vol.3, Issue 1, Feb. 1978.

[10] KHETAN, R.P. and CHIANG, F.P., "Strain Analysis by One-beam Laser Speckle Interferometry. 1: Single Aperture Method", *Applied Optics*, Vol. 15, No. 9, pp 2205-2215.

[11] BLOOMFIELD, P., *"Fourier Analysis of Time Series : An Introduction"*, Wiley series in probability and mathematical statistics, John Wiley & Sons, Inc., New York, 1976.

List of Figures

speckle pattern

laser

X-Y stage

motor controller

image plane

x_1

x_2

U_1

U_2

Laser
beam

speckle
pattern

L

S

Young's fringes in
diffraction halo

Bright fringes appear when :

$\bar{u}.\bar{d} = n\lambda L, \quad n = 0, \pm1, \pm2, \ldots\ldots$

Displacement $= |\bar{d}| = \dfrac{\lambda L}{S}$

Figure 1: Pointwise Reading of a Specklegram

23
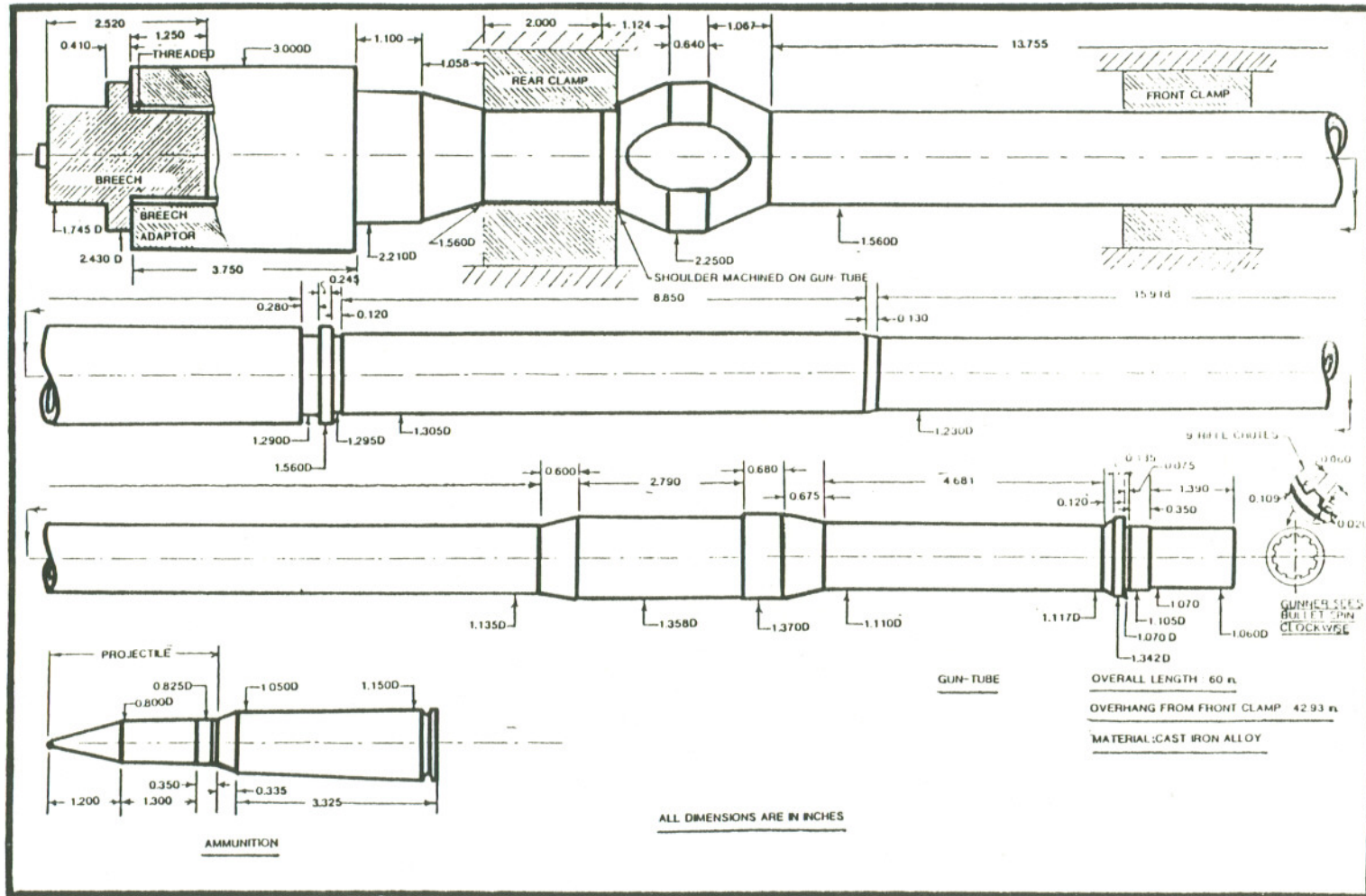
Figure 2: Dimensions of the Gun-tube
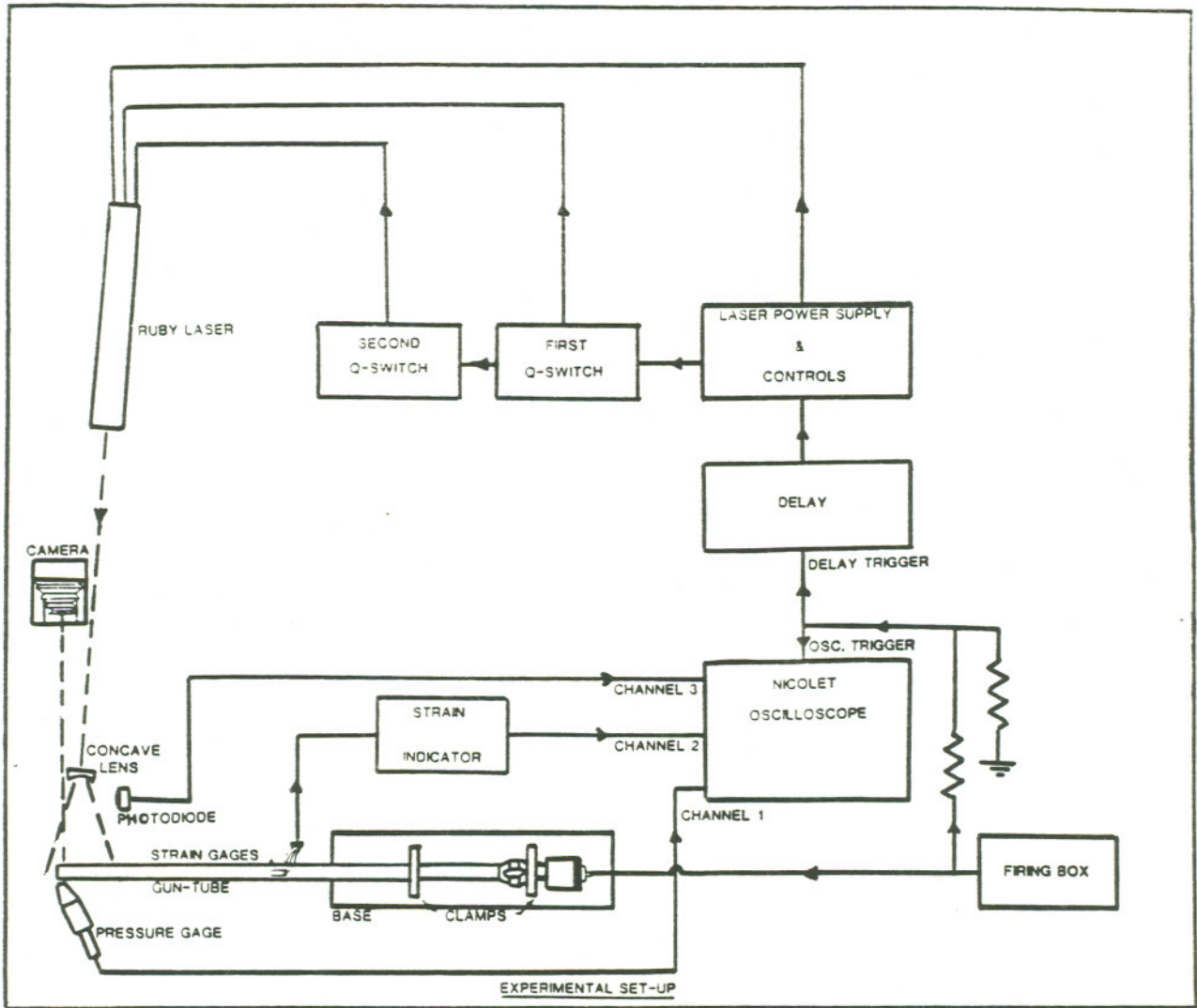
Figure 3: The Experimental Setup
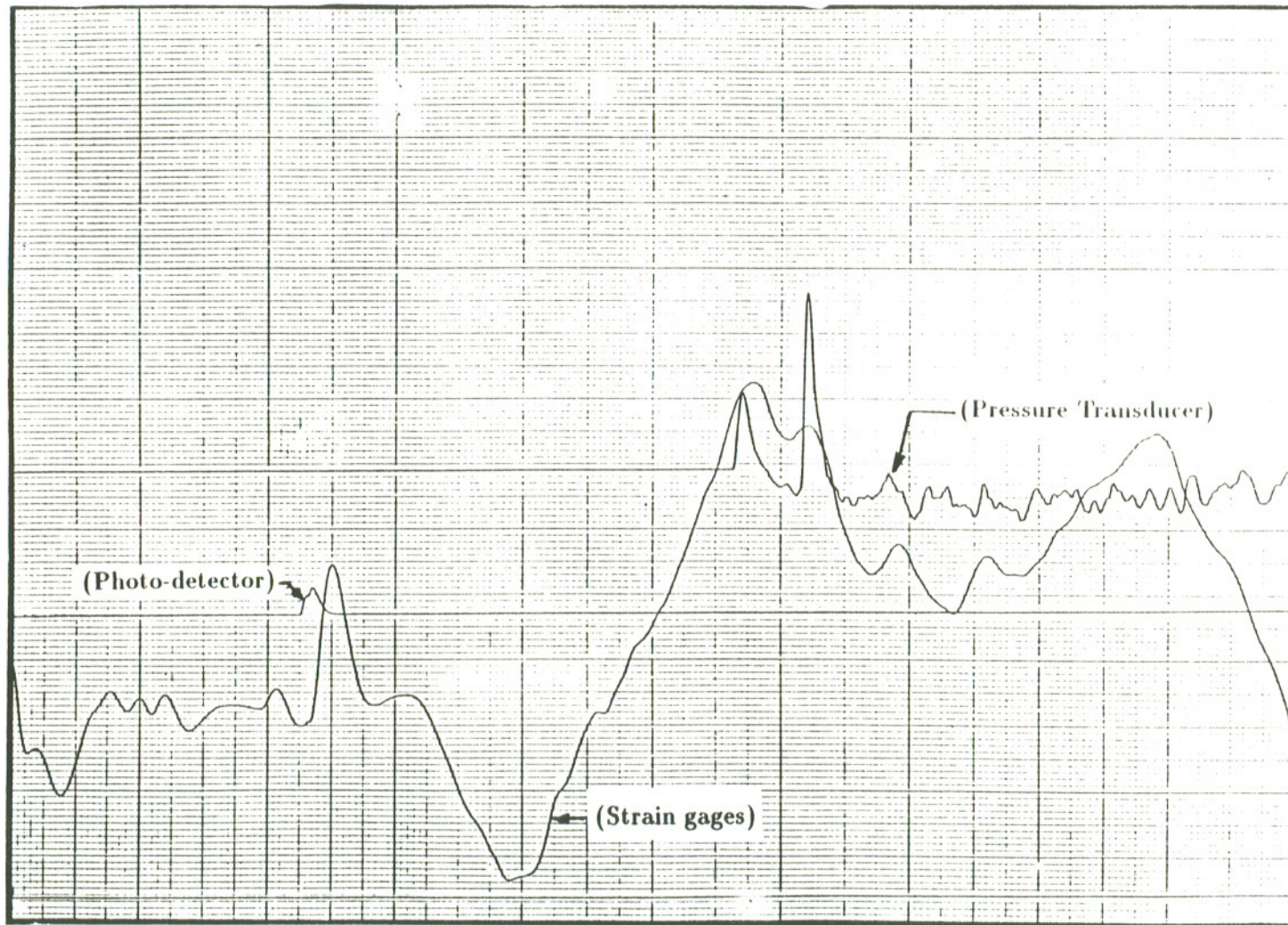
Figure 4: A Typical Oscilloscope Recording Showing Signals from the Strain
Gages, Pressure Transducer and the Photo-detector
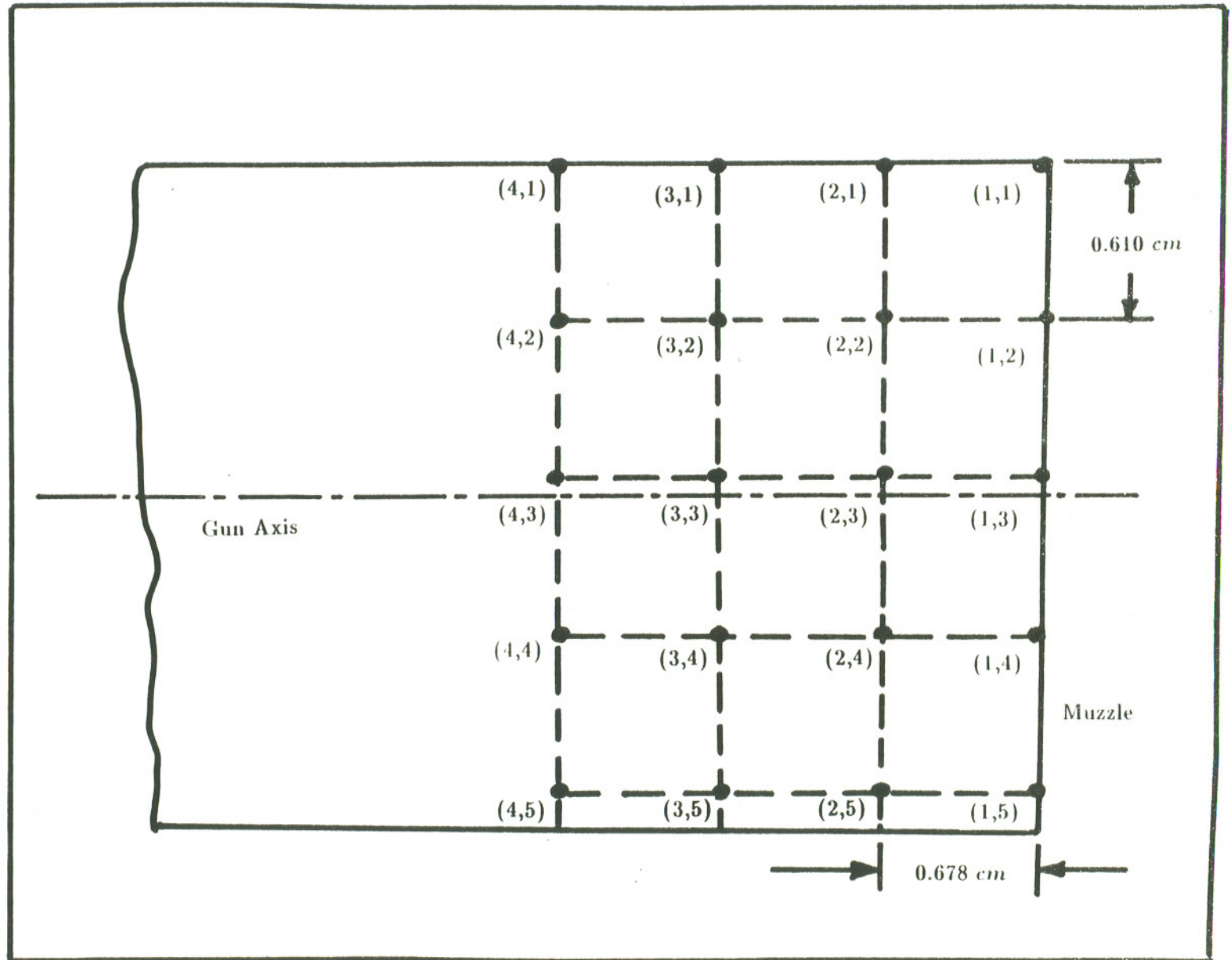
Figure 5: Location of the Points at which the Specklegrams are Analyzed

Point(4,1) Point(3,1) Point(2,1) Point(1,1)

Point(4,2) Point(3,2) Point(2,2) Point(1,2)

Point(4,3) Point(3,3) Point(2,3) Point(1,3)

Point(4,4) Point(3,4) Point(2,4) Point(1,4)

Point(4,5) Point(3,5) Point(2,5) Point(1,5)
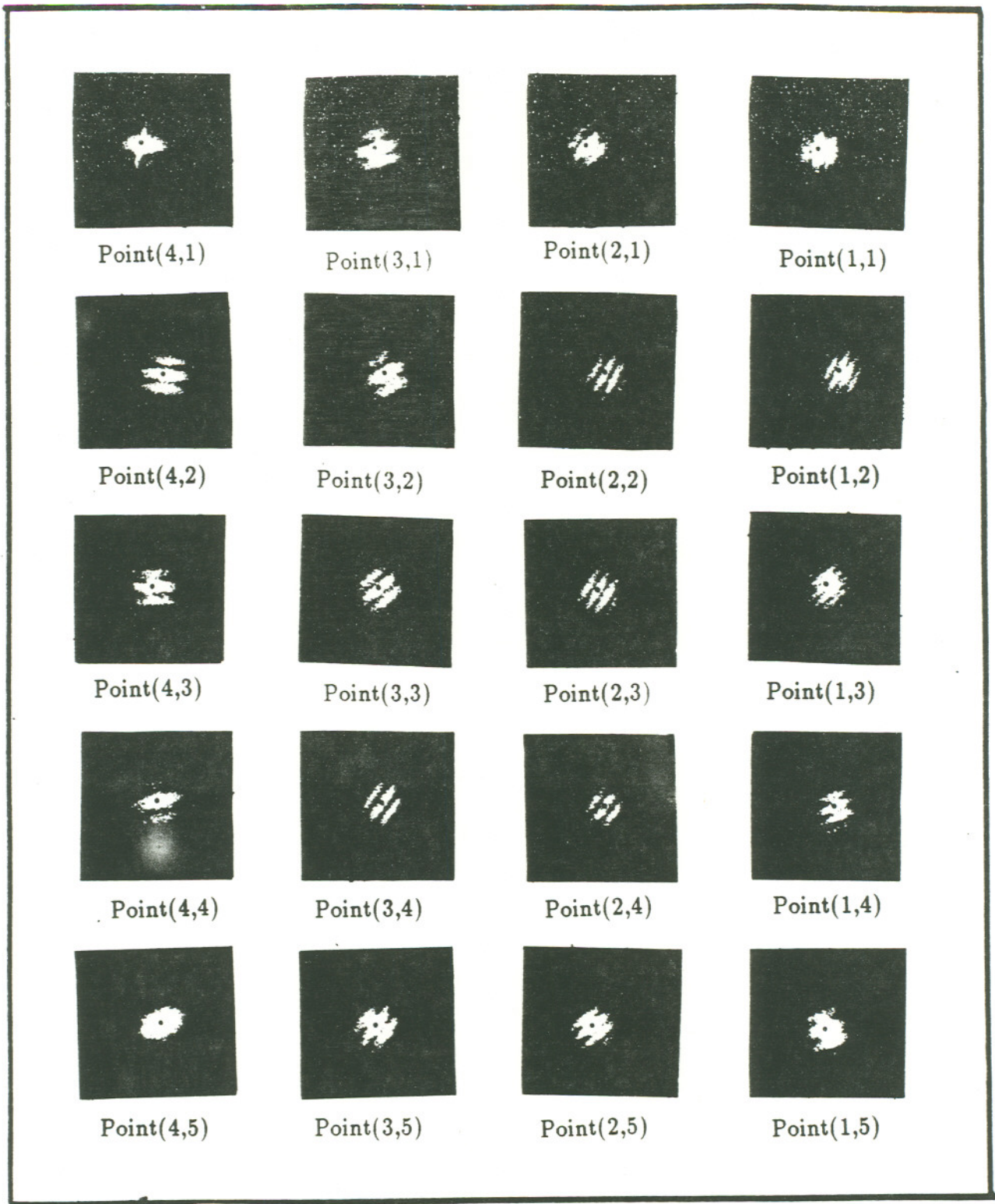
Figure 6: Young's Fringes at the Gun-tube Muzzle (Pointwise Filtering)
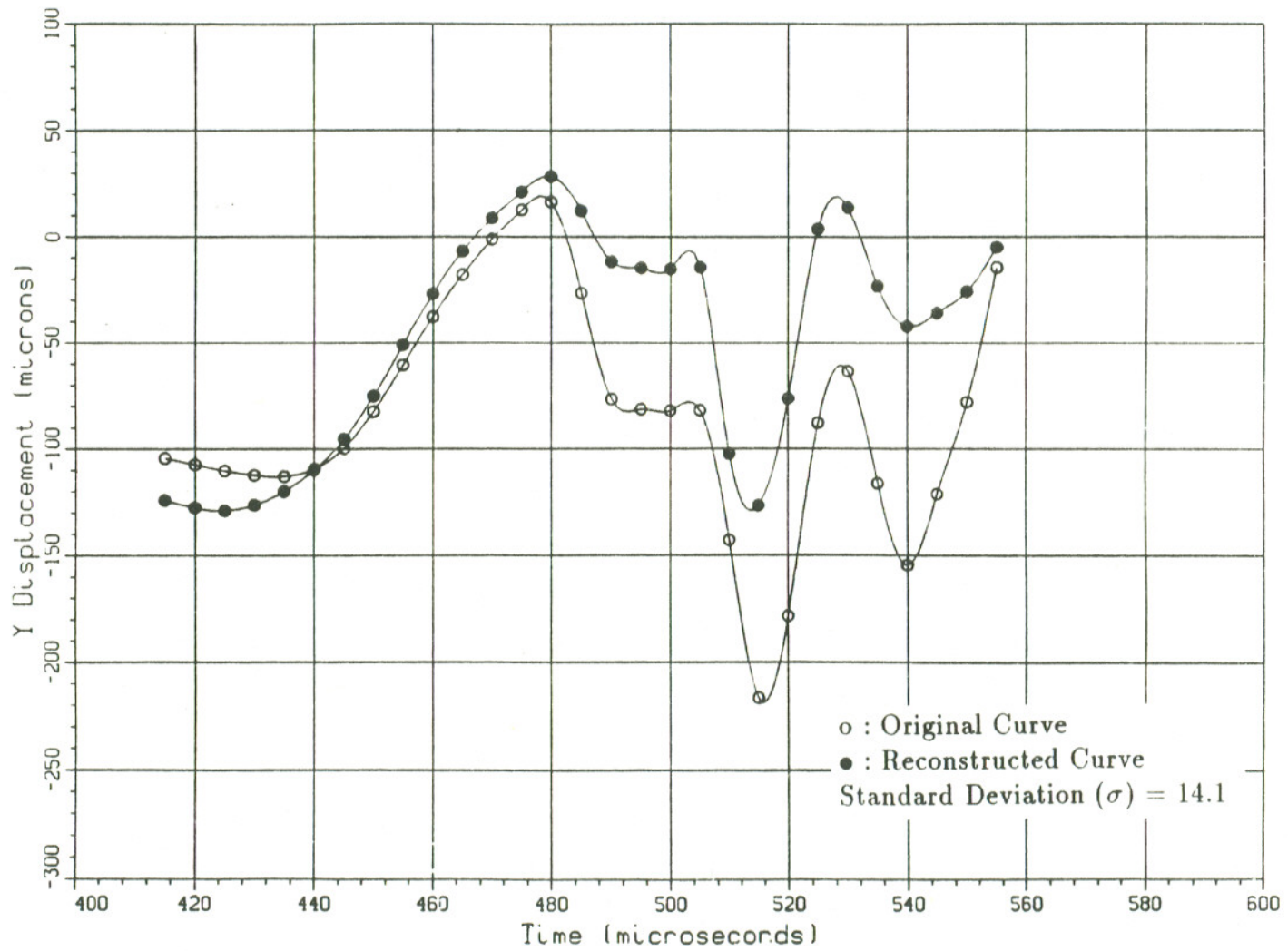
Figure 7: Interpolation Error
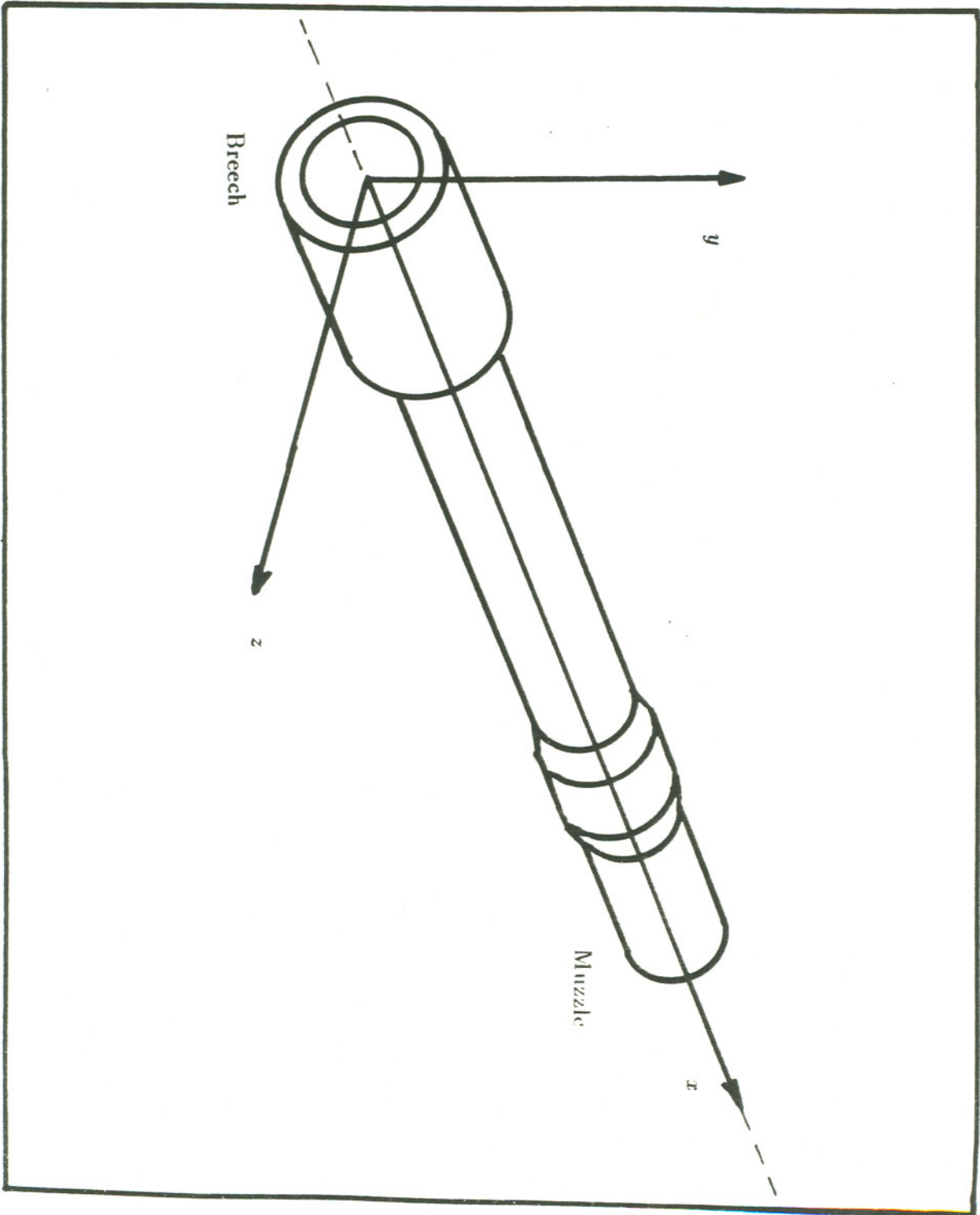
Figure 8: Location of the Coordinate System
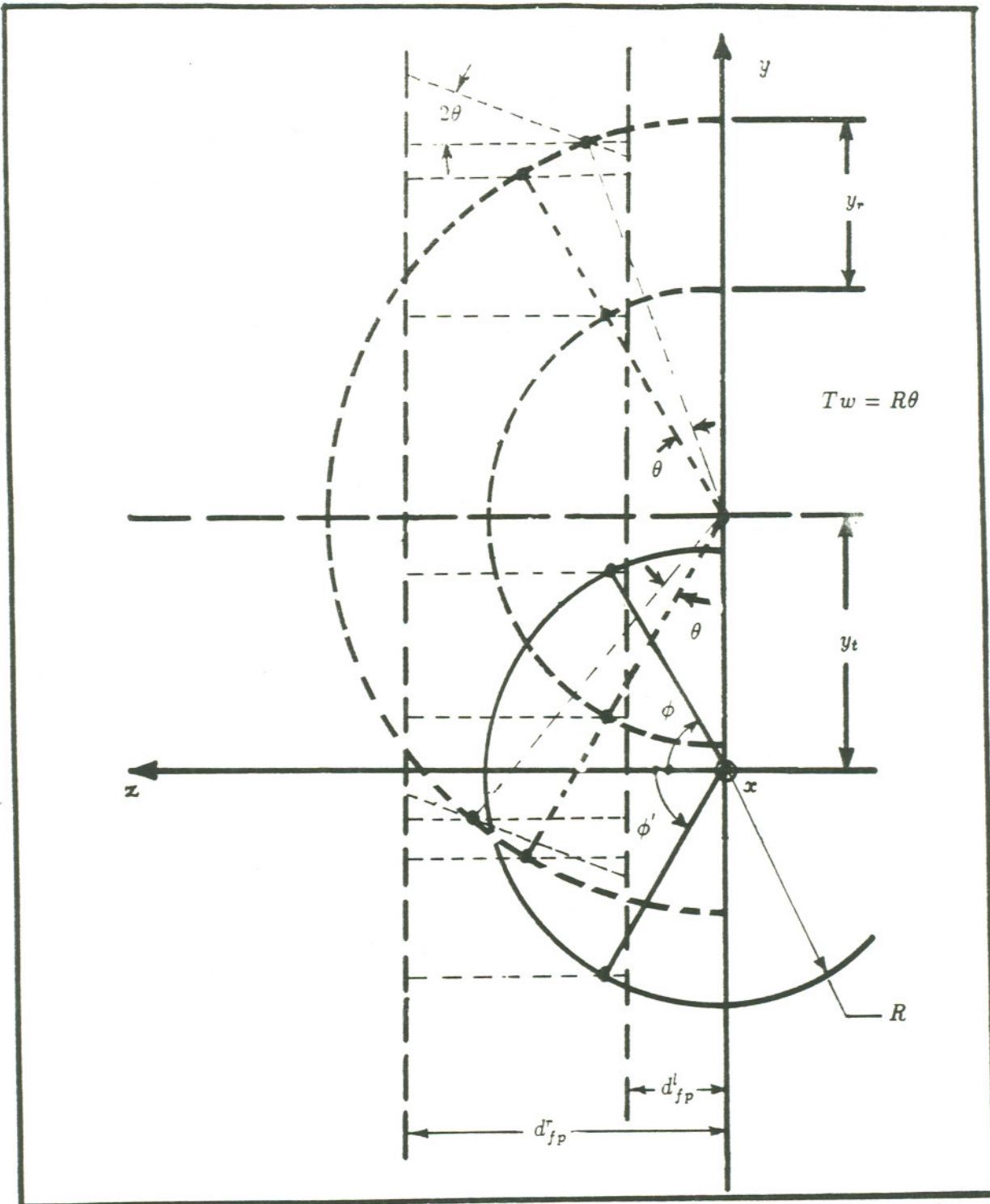
Figure 9: Speckle Displacement at the Plane at which the Camera is Focused
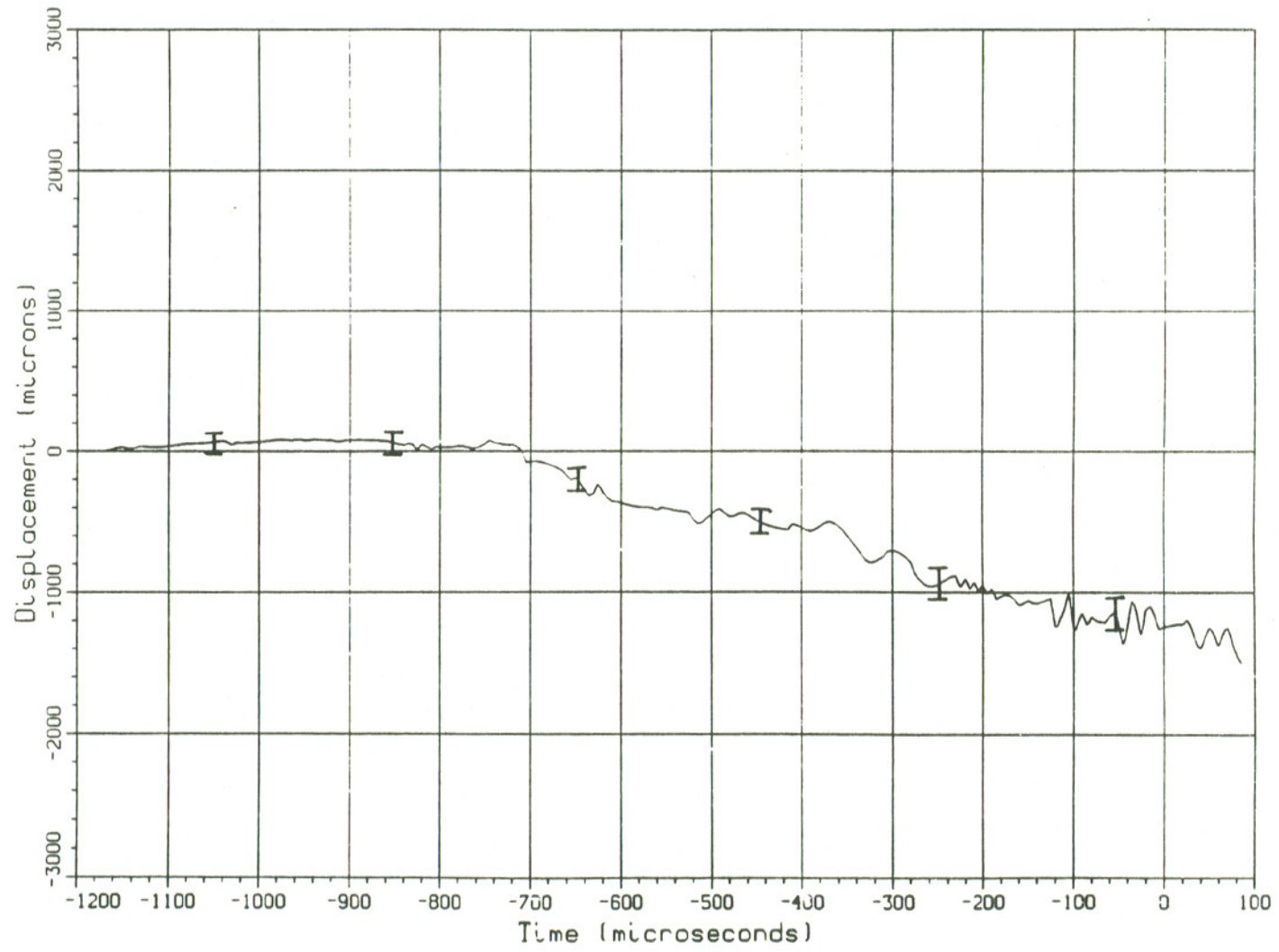
Figure 10: Transverse Displacement at Points $(1,j)$

32
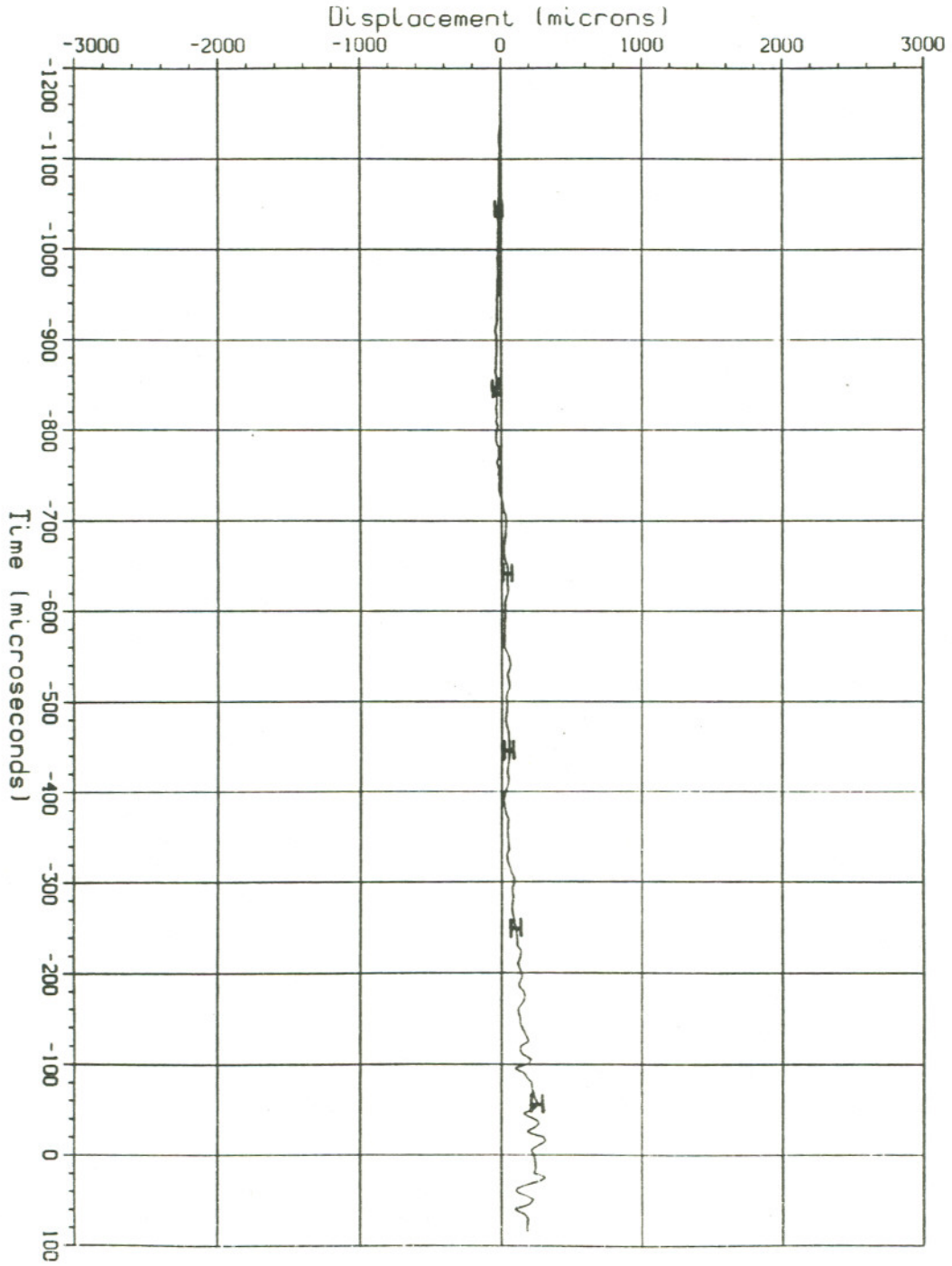
Figure 11: Radial Expansion at Points (1,j)
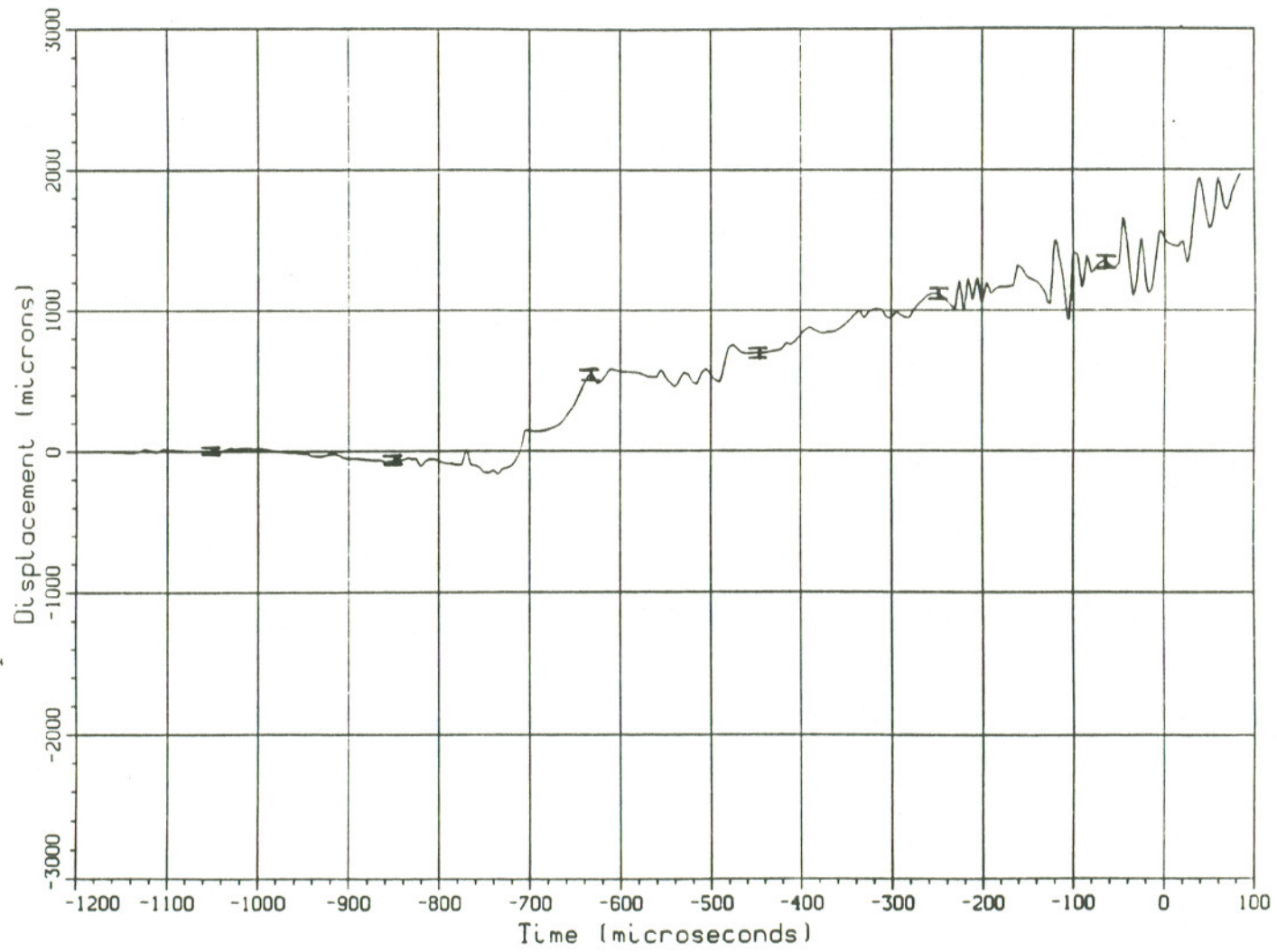
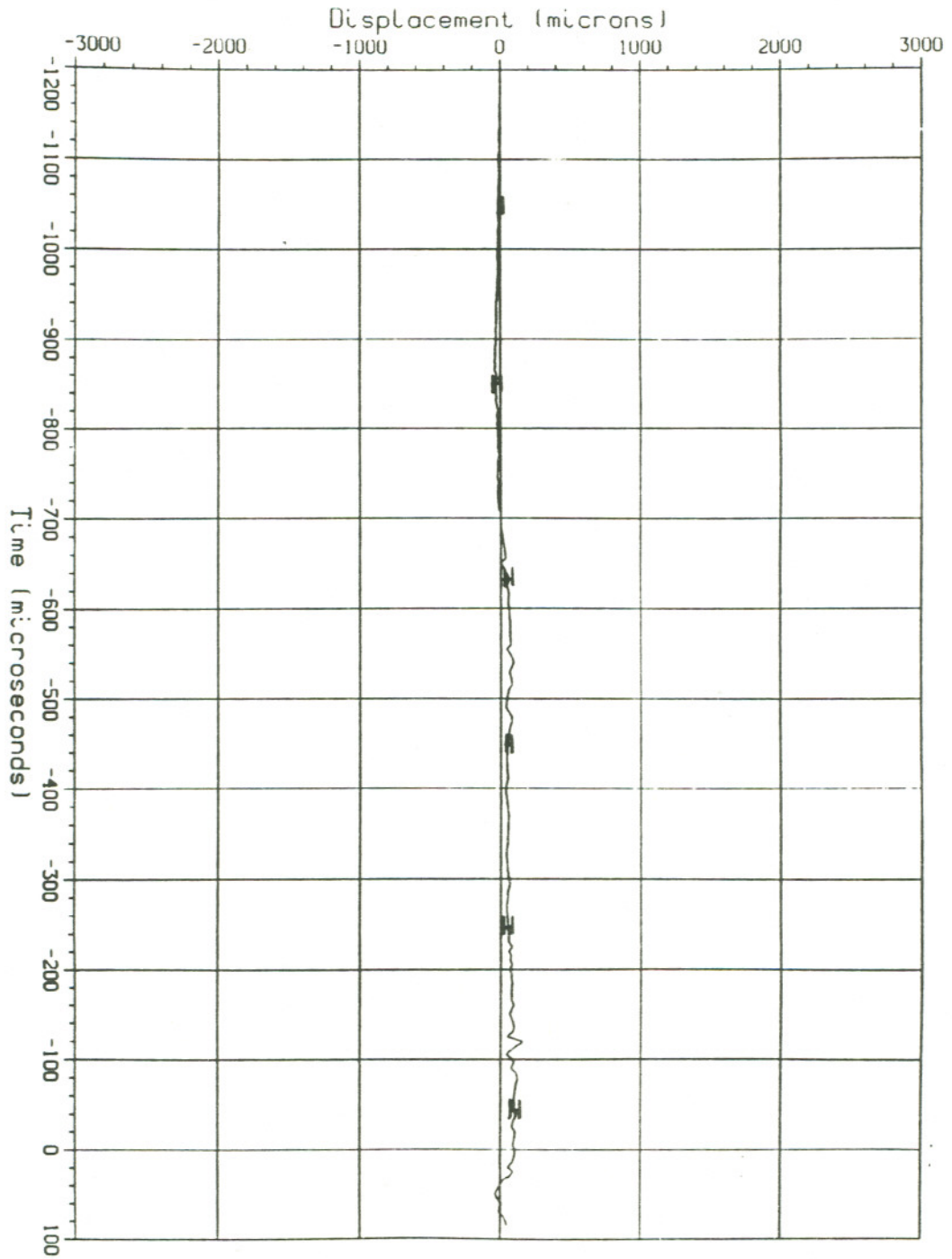Figure 12: Displacement at Surface due to Twist at Points (1,j)
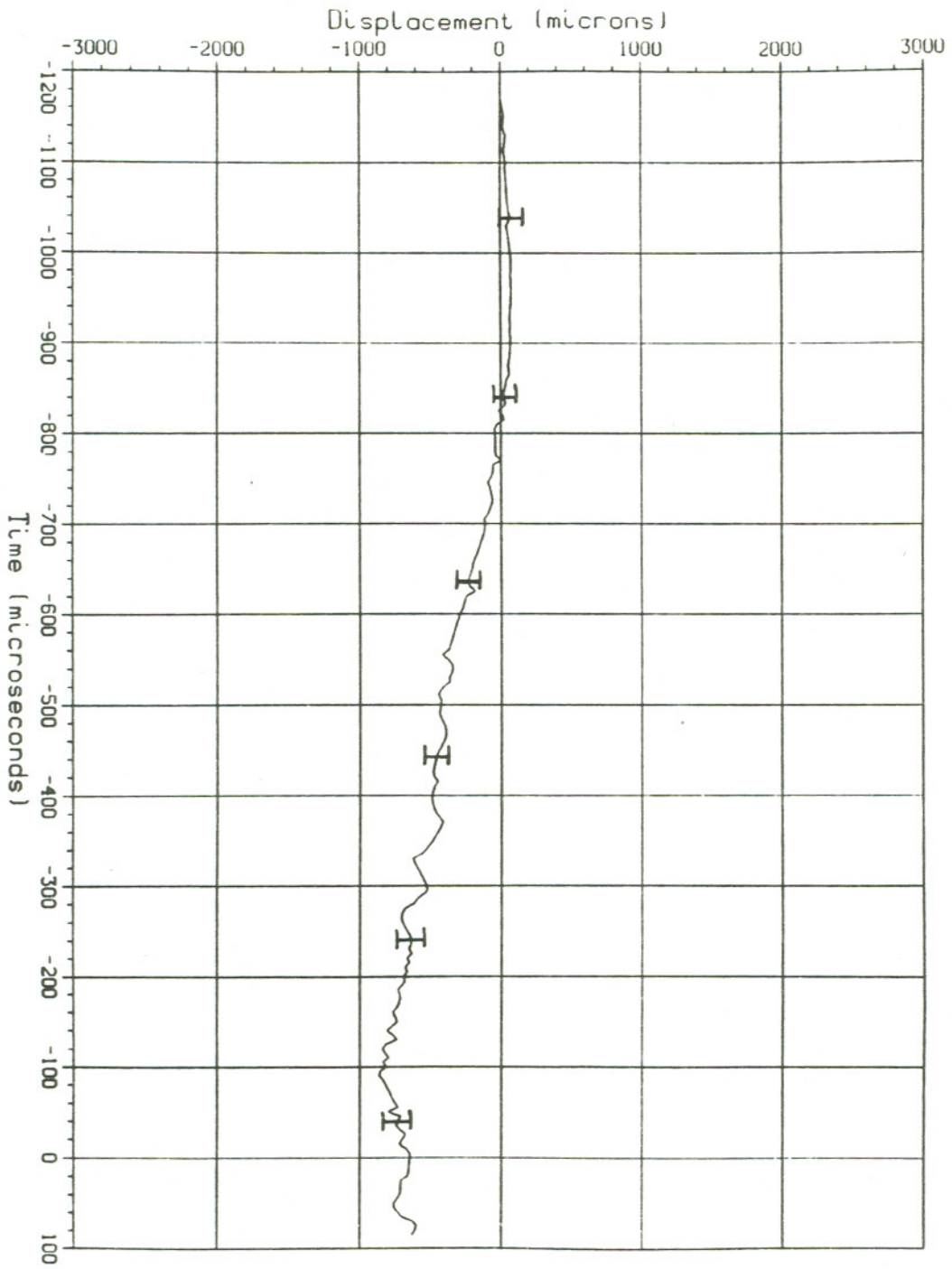
Figure 13: Transverse Displacement at Points (2,j)
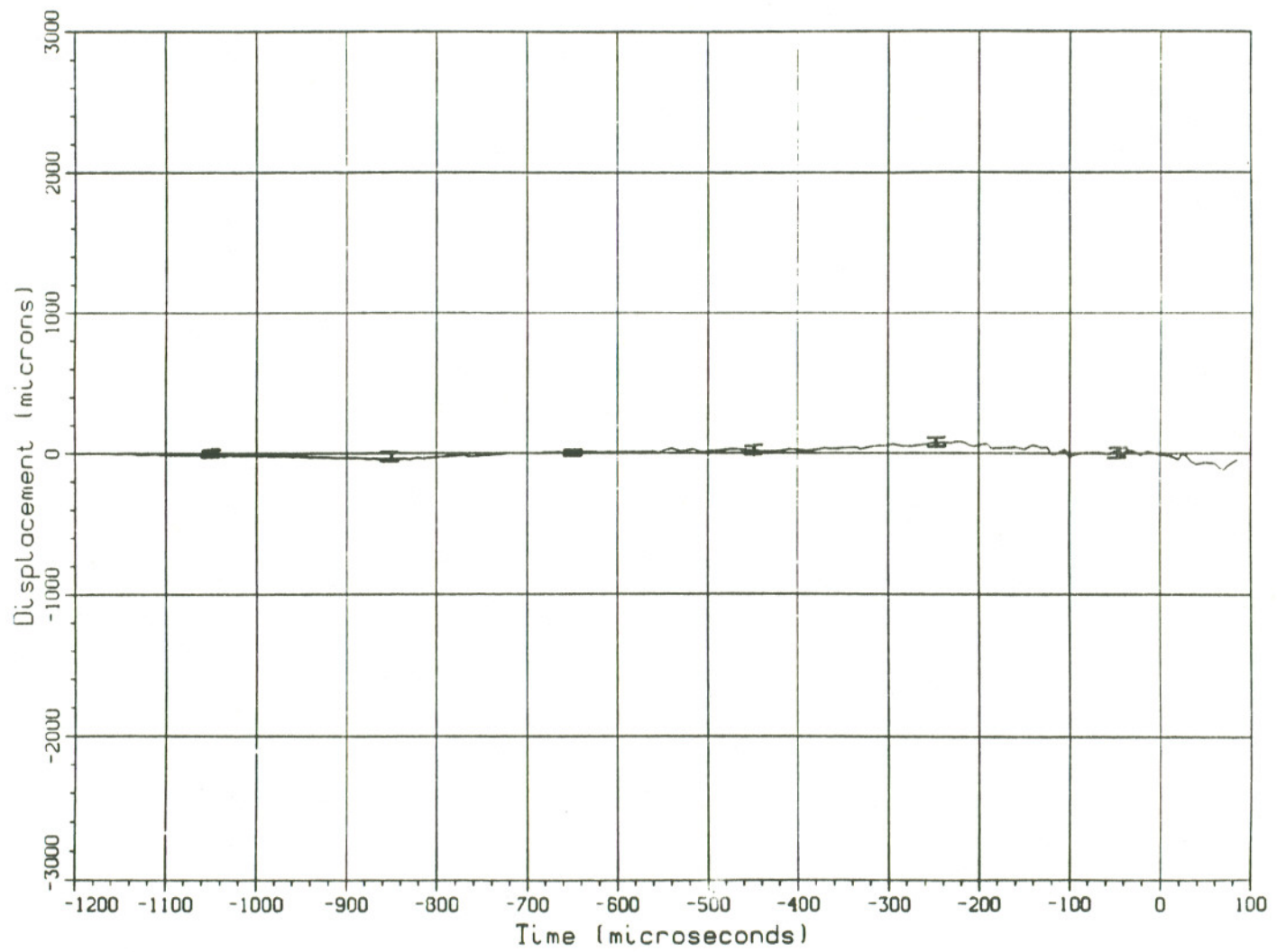
Figure 14: Radial Expansion at Points $(2,j)$
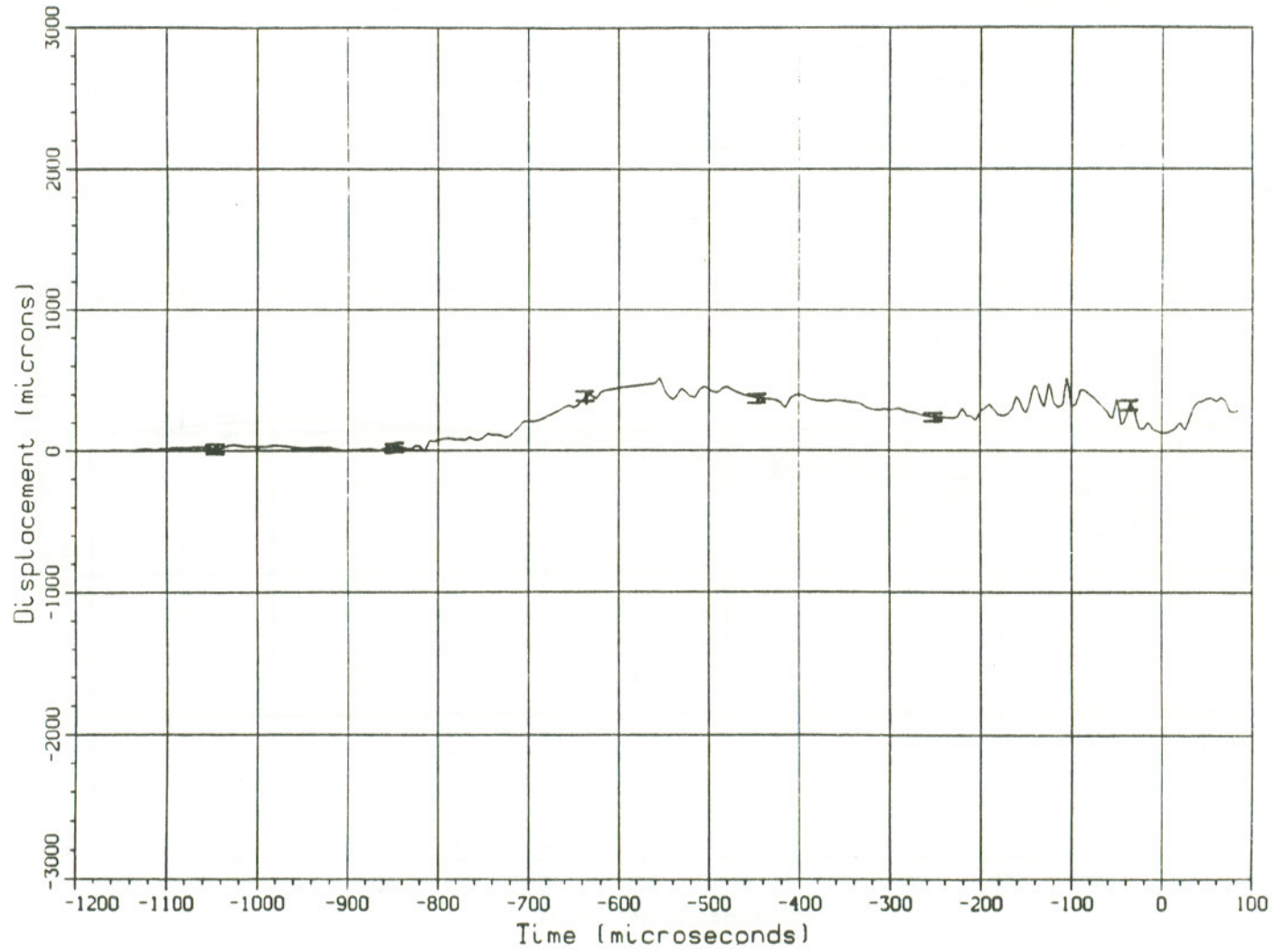
Figure 15: Displacement at Surface due to Twist at Points $(2,j)$

Figure 17: Radial Expansion at Points (3,*j*)
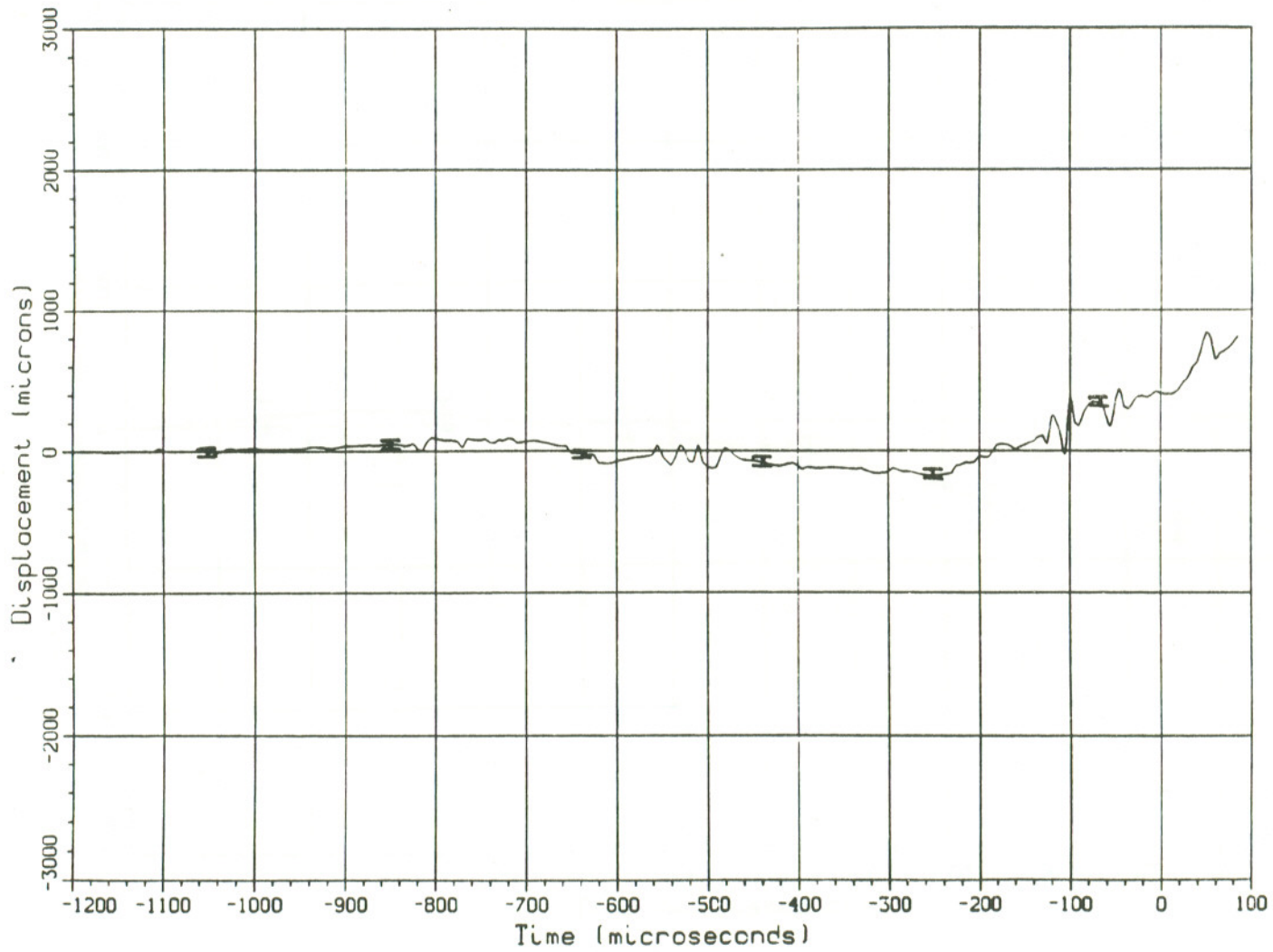
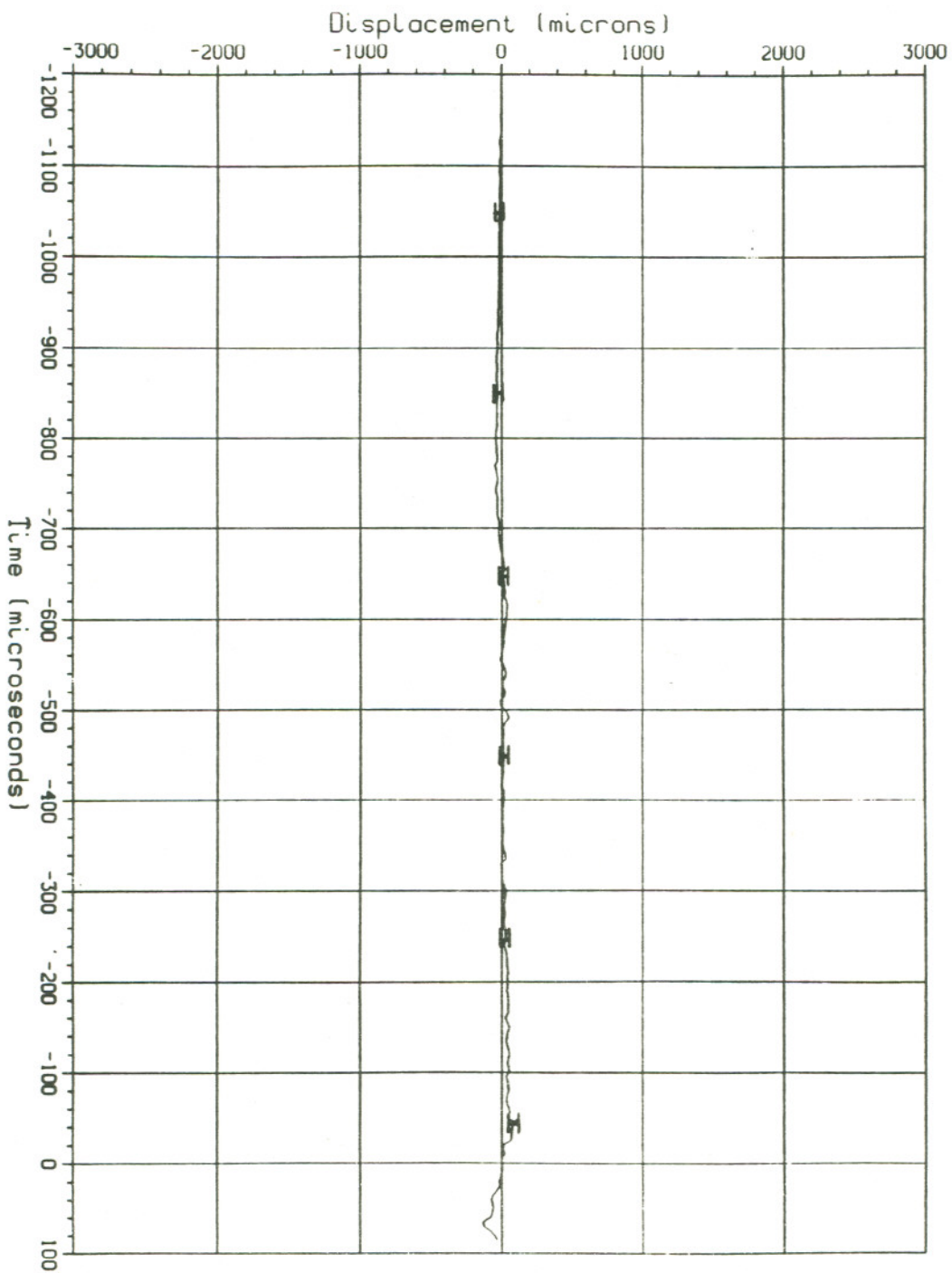Figure 18: Displacement at Surface due to Twist at Points (3,*j*)

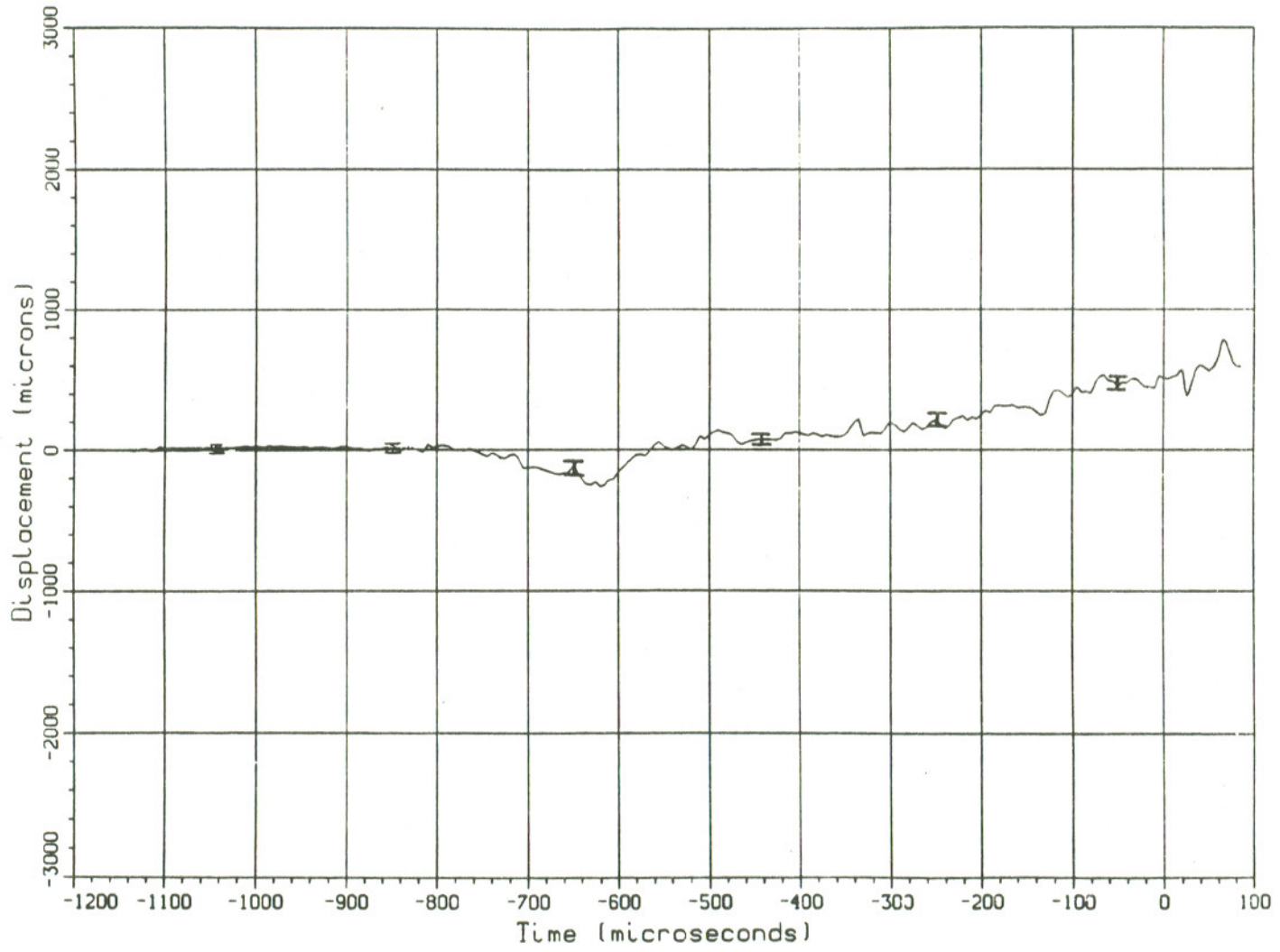Figure 20: Radial Expansion at Points (4,j)
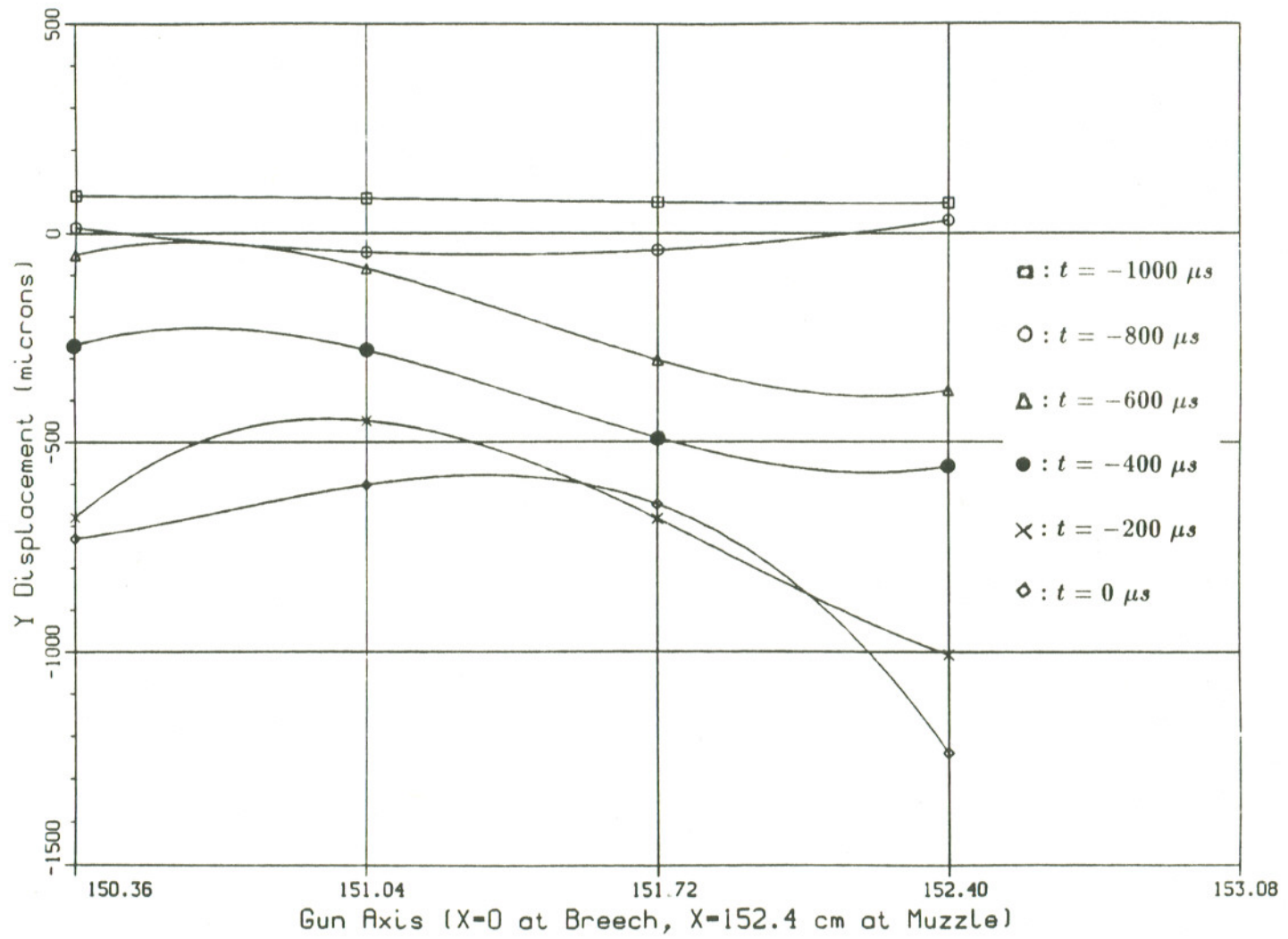
Figure 21: Displacement at Surface due to Twist at Points $(4,j)$

Figure 22: Transverse Mode Shapes at Muzzle at Various Instants